Co-delivery of Cu(I) chelator and chemotherapeutics as a new strategy for tumor theranostic

Tao Sun, Guangping Zhang, Zhongyuan Guo, Qinjun Chen, Yujie Zhang, Yongchao Chu, Qin Guo, Chao Li, Wenxi Zhou, Yiwen Zhang, Peixin Liu, Hongyi Chen, Haijun Yu, Liping Jiang, Chen Jiang

PII: S0168-3659(20)30113-9

DOI: https://doi.org/10.1016/j.jconrel.2020.02.023

Reference: COREL 10176

To appear in: *Journal of Controlled Release*

Received date: 23 December 2019

Revised date: 6 February 2020

Accepted date: 12 February 2020

Please cite this article as: T. Sun, G. Zhang, Z. Guo, et al., Co-delivery of Cu(I) chelator and chemotherapeutics as a new strategy for tumor theranostic, *Journal of Controlled Release* (2020), https://doi.org/10.1016/j.jconrel.2020.02.023

Co-delivery of Cu(I) Chelator and Chemotherapeutics As A New Strategy for Tumor Theranostic

Tao Sun[a], Guangping Zhang[b], Zhongyuan Guo[a], Qinjun Chen[a], Yujie Zhang[a], Yongchao Chu[a], Qin Guo[a], Chao Li[a], Wenxi Zhou[a], Yiwen Zhang[a], Peixin Liu[a], Hongyi Chen[a], Haijun Yu[c], Liping Jiang[d], and Chen Jiang[a,*]

[a]Key Laboratory of Smart Drug Delivery (Ministry of Education), Minhang Hospital, State Key Laboratory of Medical Neurobiology and MOE Frontiers Center for Brain Science, Institutes of Brain Science, Department of Pharmaceutics, School of Pharmacy, Research Center on Aging and Medicine, Fudan University, Shanghai 201203, PR China

[b]Shandong Province Key Laboratory of Medical Physics and Image Processing Technology, School of Physics and Electronics & Institute of Materials and Clean Energy, Shandong Normal University, 1 University Road, Jinan, 250358, PR China

[c]State Key Laboratory of Drug Research & Center of Pharmaceutics, Shanghai Institute of Materia Medica, Chinese Academy of Sciences, Shanghai 201203, PR China

[d]State key Laboratory of Molecular Engineering of Polymers, Department of Macromolecular Science, Fudan University, Shanghai 200438, PR China

Corresponding author: Prof. Chen Jiang, E-mail: jiangchen@shmu.edu.cn

Graphical abstract

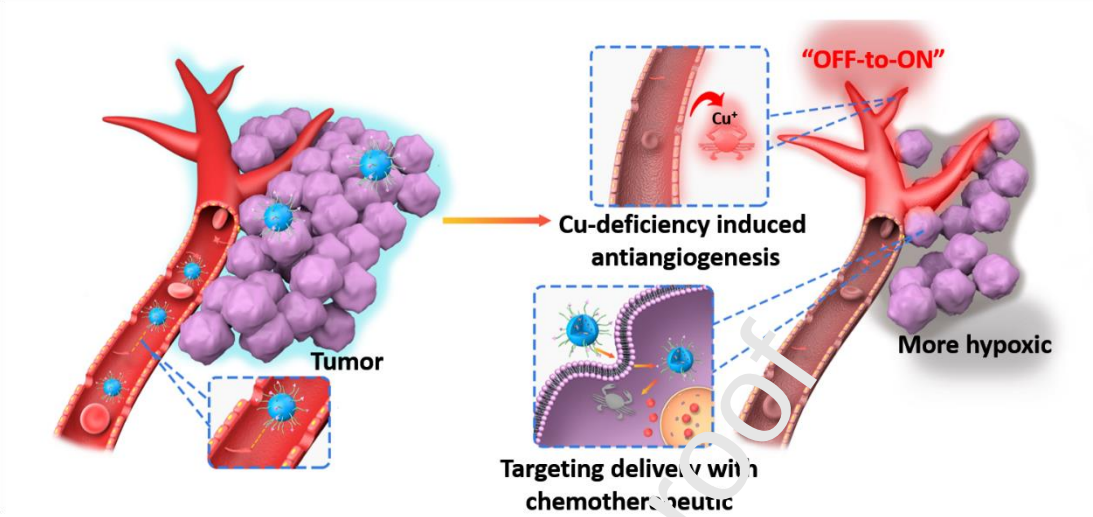

Highlights

- A theranostic specific Cu^{+} chelator was proposed.
- Targeting micelle co-loaded with Cu^{+}-chelator and chemotherapeutic reagents was fabricated.
- Antiangiogenesis and tumor's oxygen saturation reduction were reduced.
- Fine antitumor efficacy was achieved with low side effect.

ABSTRACT: Chelating Cu from tumors has been verified as an effective and promising strategy for cancer therapy through antiangiogenesis. However, systematic removal Cu by injecting with Cu chelators will result unavoidable side effects, since Cu is indispensable to the body. In this work, a micelle targeting to tumors' newborn vessels based on a polypeptide was developed to co-load DOX and Probe X, which can go through an "OFF-to-ON" procedure to report the Cu^{+}-capture events *in vivo* in a real-time way by giving near infrared (NIR) fluorescence and photoacoustic signal. By co-delivering antiangiogenesis and chemotherapeutic reagents, the tumor can be significantly suppressed, meanwhile with a low systematic toxicity. Hopefully, this work can offer new insights in designing sophisticated antitumor strategy.

Keywords

Cu chelator; Antiangiogenesis; Theranostic; Real-time reporting; Co-delivery

1. Introduction

Cu concentration, which is found extraordinarily elevated in many types of tumor, often correlates with tumor burden and recurrence [1–2]. Plentiful research suggests that Cu can promote the proliferation and migration of endothelial cells among the tumor sites [3], and Cu is also indispensable for tumor cells to secrete angiogenic factors [4]. There are already research on animal models focusing on suppressing tumor angiogenesis direct by inhibiting *in vivo* copper trafficking [5]. A famous case under clinical trial is tetrathiomolybdate, a strong copper chelator, which has been proved able to suppress angiogenesis and tumor growth *via* copper deficiency [6].

Chelating Cu can remarkably lower Cu concentration systematically by promoting the excretion after chelating [7]. However, Cu is a required element for life and an essential element functionalizing in most aerobic organisms, mainly playing as a structural and catalytic cofactor, and consequently involved in many biological pathways. Notably, lowering the Cu concentration systematically by simply injecting with Cu chelators was already found to cause severe side effects, including erythra, optic neuritis, emesis and leucopenia [8]. From another perspective, without enough reliable information on "when, where, how and how much" of the chelators' fictionalization, clinical medication could be implicit [9]. As to our knowledge, there are very few reported systems concerning chelating Cu *in vivo* meanwhile with a reporting system [10]. It remains challenging to integrate a specific drug carrier to deliver Cu chelators to tumors to avoid systematic toxicity and meanwhile provide the real-time information on pharmacodynamics.

Cu, especially its monovalent form Cu^{+}, serves as a critical signaling species in cells and can function in multiple organelles of tumor cells [11–12]. Cu^{+} plays a more important role than Cu^{2+} in tumor development and metastasis. On the other hand, in tumors' reducing microenvironment, Cu can stay in the Cu^{+} state [13] and be stabilized with GSH or Vitamin C within the cytosol [14]. Removal of Cu^{+} is more direct and Cu concentration will be thus synchronously lowered through the redox balance of Cu^{+}-Cu^{2+} [15].

From both clinic and theory, the synergistic therapy of chemotherapy and

antiangiogenesis is reasonable, where chemotherapy directly kills tumor cells and antiangiogenesis modulates the microenvironment by reducing new vessels that support tumors [16]. In clinic, there are already attempts trying to combine chemotherapy and antiangiogenesis together to suppress the cancer progress [17], while the clinical therapeutic efficacy by using combinations (such as bevacizumab/5-fluorouracil and trastazumab/paclitaxel for treating metastatic colorectal/breast cancers) has been well approved [18]. However, it is still challenging in specifically delivering chemotherapeutic agents and Cu chelators to the tumor sites for better synergy, since they often perform greatly different physical properties. The strategy can be further pushed forward by the targeting nanomedicine technology with finer efficacy and improved biocompatibility.

In this work, we co-loaded DOX and a Cu^+ Probe 1 (both as the chelator and tracer) into a micellar system built from a body-friendly polypeptide amphiphile (Scheme 1 and Figure 1). The micelle was integrated with cRGD to target tumors' neoangiogenesis, based on which, the chemotherapeutics and chelator can be delivered to tumor simultaneously. The Cu^+ chelating events can be monitored by NIR fluorescence and photoacoustic imaging in a non-invasive and real-time way. After treatment, Cu level and oxygen saturation were significantly down-regulated in tumors, and the antineoangiogenesis mechanism was studied. The improved combined anti-tumor efficacy from antiangiogenesis and chemotherapy was achieved. Finally, the *in vivo* toxicity was also investigated. These findings, hopefully, can provide new insights to design, fabricate and tailor artificial antitumor nanosystems.

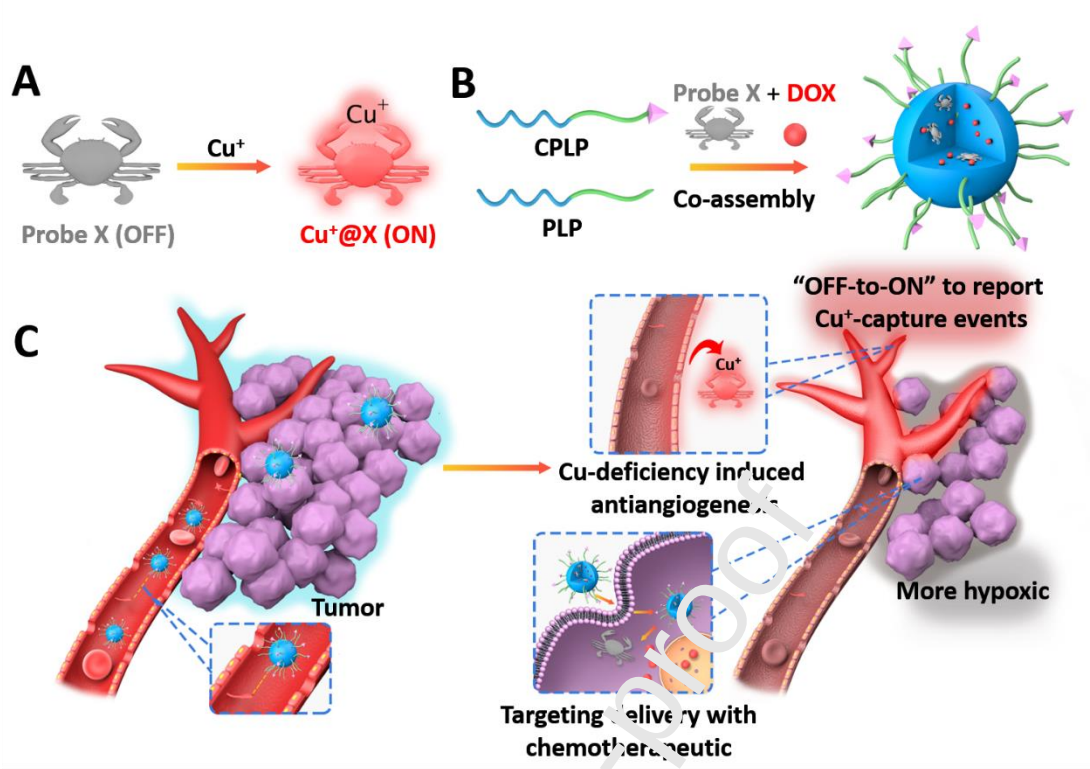

Scheme 1. Illustration of the co-delivery of Cu^+ chelator and chemotherapeutics as a new strategy for tumor theranostic. (A) "OFF-to-ON" procedure of Probe X induced by the specific molecular recognition with Cu^+; (B) Targeting micelle co-assembled from CPLP/PLP/Probe X/DOX, (C) the tumor-targeting delivery (EPR effect and cRGD receptor) and tumor theranostics mechanism.

2. Materials and methods

2.1 Materials

N_3-PEG-NH_2 (MW 5000) and PEG-NH_2 (MW 5000) were purchased from JenKem Technology Co. Ltd. (Beijing, China). Lys (cbz), phe, triphosgene and cyclohexanone were from Aladdin (Shanghai, China). HBr, AcOH, NaOH, NaOAc and CuI were from Energy Chemical (Shanghai, China). Thiourea, $POCl_3$, ethyl 2-hydroxyethyl sulfide, PMDETA and VcNa were commercially available from Sigma-Aldrich (Shanghai, China). Deuterium reagents for nuclear magnetic resonance (NMR) spectroscopy including $CDCl_3$ and DMSO-δ_6, CD_3OD and D_2O were from J&K Scientific Ltd. (Beijing, China). All other chemicals and mentioned solvents were from Sinopharm Chemical Reagent (Shanghai, China). Thin layer chromatography

(TLC) boards and silica gel for column (SilicaFlash F60, 230~400 mesh) were from Haiyang Chemical (Qingdao, China), while Ar was from Lyumin Gas Co. Ltd. (Shanghai, China). cRGD-alkyne was purchased from China Peptide (Hangzhou, China). Dulbecco's modified Eagle's medium (DMEM) and fetal bovine serum (FBS) were from Gibco BRL (Carlsbad, CA, USA). Nonessential amino acids, trypsin-EDTA (0.25%), streptomycin, and penicillin were from Invitrogen Co. (Waltham, Massachusetts, USA). Dialysis bags and filter membrane were from Amicon Ultra (Millipore, MA, USA).

2.2 Equipment

^{1}H NMR spectra were undertaken on Varian Oxford NMR spectrometer (400 MHz, Palo Alto, CA, USA) at room temperature. ^{13}C NMR spectra were recorded on Bruker NMR Ascend spectrometer (600 MHz, Billerica, MA, USA) at room temperature. FT-IR spectra were obtained employing ATR geometry on a Perkin-Elmer infrared spectrophotometer (Waltham, MA, USA) at room temperature. Electron spray ionization mass spectrometry (ESI-MS) was from Agilent LCMSD (Santa Clara, CA, USA). Transmission electron microscopy (TEM) images were carried on a JEM-100CX electron microscope from JEOL Ltd. (Tokyo, Japan). DLS and ζ-potential results were obtained from a Wyatt QELS Technology DAWN HELEOS instrument (Santa Barbara, CA, USA) a 12-angle replaced detector in a scintillation vial and a 50 mW solid-state laser operated at 25 ^{o}C. Chemical structures were drawn on ChemBio 3D Ultra (14.0 version, Cambridge Soft-ware, MA, USA). Chemical quantification was carried out on an analytical HPLC (Agilent Technologies Inc., CA, USA), equipped with gradient flow control pump (1260 Quat Pump-G1311B), auto-sampler (1260 ALS-G1329B), diode array detector (1260DAD-G4212B), fluorescence detector (FLD-G1321A), column oven (1290 TCC-G1316C) and a 250-4.6 mm column (reversed phase-C18 (5 mm), Agilent Technologies Inc., CA, USA). Cells were observed on a fluorescence microscope (Leica, Wetzlar, Germany). Small animal *in vivo* fluorescence imaging was photographed on a Molecular Biology Workstations (Image Visualization and Infrared Spectroscopy, IVIS, Caliper, Newton,

MA, USA). Cu concentration in tumors was determined by Inductively Coupled Plasma-Mass Spectrometry (ICP-Ms, Varian, Palo Alto, CA, USA) authorized to National Center of testing Technology (Shanghai, China).

2.3 Synthesis

2.3.1 Synthesis and characterizations of the amphiphilic polypeptide

Peptide monomers: Lys (cbz)-NCA and phe-NCA were synthesized *via* the classic Fuchs-Farthing method using triphosgene [19]. Briefly, lys (cbz) (3 g, 10.7 mmol) and triphosgene (1.27 g, 4.28 mmol) in anhydrous THF (30 mL) were stirred for 3 h at 50 ^{o}C under Ar. The mixture was cooled down to room temperature and slowly dripped into cold anhydrous cyclohexane under rigorous stirring. The suspension was allowed to crystallize at -20 ^{o}C overnight, and the appeared white solid was filtered and dried to give Lys (cbz)-NCA. Phe-NCA was obtained *via* a similar way. The ^{1}H NMR and ^{13}C NMR spectra were in accordance with the reported literature [19].

XPEG-pLys-pPhe (X=MeO or N_3). The triblock polymer XPEG-pLys-pPhe (X=MeO or N_3) contains the units of ethylene glycol (112, MW 5000), lysine (12) and phenylalanine (18), and was prepared from a ring-opening polymerization reaction (Figure 1) with XPEG-NH_2 as the initiator. To a stirred solution of XPEG (1 g, 0.2 mmol) in anhydrous DMF (10 mL), dried Lys (cbz)-NCA (736 mg, 2.4 mmol) from the last step was added and maintained under stirring at 50 ^{o}C under Ar for 48 h. Then Phe-NCA (1.15 g, 6 mmol) in anhydrous DMF (20 mL) was injected into the suspension cooled to room temperature, and the mixture was maintained at 50 ^{o}C under Ar for another 48 h. Then the suspension was cooled to room temperature and slowly dripped into cold diethyl ether to allow the precipitation (×3). The white solid was filtered and isolated by repeated precipitation from DMF into XPEG-*p*Lys (cbz)-*p*Phe, which was then treated with a mixed solvent of TFA (10 mL) and HBr/HOAc (0.5 mL, 5wt HBr%) for 3 h at room temperature to deprotect the cbz groups on lysine. The acidic solution was precipitated thrice in diethyl ether, redissolved into pure water (5 mL) and dialyzed against water with a membrane

(MWCO 1000) for 24 h (It should be noted that if the acidic solution was directly treated with a dialysis against water, possible hydrolysis of the polypeptide could occur catalyzed by residual acid in the dialysis bag.). Then the solution in the bag was freeze-dried to give XPEG-*p*Lys-*p*Phe.

cRGD-PEG-pLys-pPhe: cRGD was coupled onto the terminus of N_3-PEG-*p*Lys-*p*Phe *via* a Click reaction catalyzed by CuI. cRGD-alkyne (5 eq) and N_3-PEG-*p*Lys-*p*Phe (1 eq) were dissolved in anhydrous DMF under Ar. A solution of CuI (0.05 eq), sodium ascorbate (10 eq), and PMDETA (1 eq) in anhydrous DMF was injected into the mixture, which was stirred at room temperature at dark under Ar for 12 h. The solution was finally dialyzed against EDTA aqueous solution (10 mM, 48 h, to remove Cu^+ and Cu^{2+}) and then deionized water (48 h) using a membrane (MW 1000), followed by a freeze-drying to give the final product cRGD-PEG-*p*Lys-*p*Phe.

2.3.2 Synthesis and characterizations of Cu^+ chelator

3,6,12,15-Tetrathia-9-monoazaheptadecane (Compound 2): Compound 2 was synthesized following a reported literature [20], and the characterizations were all in accordance with reported literature (Figure S1 to S8). A mixture of ethyl 2-hydroxyethyl sulfide (4.25 g, 40 mmol) and thiourea (3.05 g, 40 mmol) in hydrobromic acid (48wt%, 8.5 mL, 75 mmol) was refluxed overnight under Ar. The mixture was cooled to room temperature, and NaOH (3.2 g, 80 mmol) aqueous solution (10 mL) was added slowly. The mixture was further refluxed overnight under Ar, and then cooled to room temperature, neutralized with HCl aqueous solution (1 M), followed by an extraction with DCM (50 mL×3). The organics were combined, washed with water (100 mL) and brine (100 mL), dried over Na_2SO_4, and evaporated to dryness to harvest compound 1 as a colorless oil, which was used without purification.

The oxidizing layer of sodium lumps was carefully removed with a knife. Sodium (1.29 g, 56 mmol) and 3-thiapentan-1-thiol (4.1 g, 33.6 mmol) were suspended in

absolute ethanol (60 mL) and the resulting suspension was heated to reflux. A solution of bis(2-chloroethyl) amine hydrochloride (2.0 g, 11.2 mmol) in absolute ethanol (35 mL) was then injected into the above solution, which was then refluxed for 4 h. The mixture was cooled to room temperature and EtOH was removed under vacuum. The residual solid was carefully quenched with water in an ice-bath. DCM (150 mL) was used to extract the suspension. The organics were washed with water, dried over dried over Na_2SO_4, and evaporated to dryness to give a crude product, which was further purified with a flash column chromatography (DCM:MeOH, 50:1 to 10:1, v:v) to give compound 2 as a chocolate oil (2.3 g, 66.1%).

IR780 (Compound 5): IR780 was synthesized following a reported literature [21], and the characterizations were all in accordance. To a solution of DMF (20 mL, 273 mmol) in ice-bathed anhydrous DCM (20 mL) under Ar, $POCl_3$ (17.5 mL, 115 mmol) in anhydrous DCM (5 mL) was added dropwise in 0.5 h. Then, cyclohexanone (5 g, 50 mmol) was injected slowly into the above solution. The resulting mixture was stirred vigorously at 80 ^oC for 3 h, and poured into ice-cold water under stirring to obtain a yellowish precipitation. The solid was filtered off, washed with water, and dried under vacuum to give compound 3 (8.1 g, 93.2%) as a yellowish solid with a fine purity (Figure S9).

To a solution containing 2,3,3-trimethyl-3H-indole (2 g, 12.5 mmol) in ACN (20 mL), 1-iodopropane (10.6 mL, 62 mmol) was added, and the mixture was refluxed under stirring overnight. ACN was then removed under vacuum. The residual solid was washed with diethyl ether, air-dried and recrystallized in acetone to obtain compound 4 as a white solid (3.3 g, 80.4%).

Compound 3 (0.5 g, 2.9 mmol) and compound 4 (1.91 g, 5.81 mmol) were dissolved in BuOH-toluene (25 mL, 7:3, v:v) under Ar, and the solution was refluxed overnight in a 100-mL flask with three necks installed with a Dean-Stark condenser to remove generated water. Then, all solvents were removed under vacuum and the residual solid was purified with a flash chromatography (DCM:MeOH, 50:1 to 20:1, v:v) to give

compound 4 (IR780, 1.6 g, 85.3%) as a dark green solid.

Probe X: Probe X was synthesized following a reported literature [22], and the characterizations were all in accordance. Compound 5 (0.14 g, 0.20 mmol) and compound 2 (0.20 g, 0.80 mmol) were dissolved in anhydrous DMF (20 mL), and the mixture was maintained at dark/80 ^{o}C for 4 h under Ar. DMF was then removed under vacuum, and the resulting residual solid was purified by flash columnchromatography (DCM:EtOH, 200:1 to 20:1, v:v) to give Probe X as a dark blue solid (0.081 g, 0.18 mmol, 38.8%) with a fine purity (Figure S10).

2.4 UV-vis spectrometer for Job's plot

The complex stoichiometry of Probe X with Cu^{+} in solution (water:ACN=1:1, v:v) was determined by Job's continuous variation method using a UV-vis spectrometer. A set of working solutions were obtained by mixing Vg mL of the stock Probe X solution (10^{-4} mol/L) with (Vt-Vg) mL of the stock Probe X solution (10^{-4} mol/L), where Vt is a fixed total volume and Vg is a variable volume for guest (from 0 to 10 mL, $0 \leq Vg \leq Vt$). To obtain the complex constant, the concentration of $[Cu(MeCN)_4][PF_6]$ (2×10^{-5} mol/L) was kept constant with the concentration of Probe X ranging from 4×10^{-4} to 3.6×10^{-3} mol/L.

2.5 FT-IR spectrometer

The sample of Probe X/Cu^{+} complex for FT-IR was obtained by freeze-drying the Probe X/$[Cu(MeCN)_4][PF_6]$ (1:1, molar ratio) aqueous solution, while the physical mixture was prepared by just freshly mixing solid Probe X and $[Cu(MeCN)_4][PF_6]$ (1:1, molar ratio) together. Notably, during grinding with KBr for the FT-IR cake, the molecular recognition between Probe X/Cu^{+} could occur, so solid Probe X and $[Cu(MeCN)_4][PF_6]$ should be grinded with dry KBr separately, mixed together rapidly and tableted into a single cake before measurement to minimize the unexpected complexion.

2.6 Geometric optimization

In order to verify the possibility of the molecular recognizing mechanism model, a geometric optimization was performed and the result was shown in the supporting video. Atomic-based simulation can play a useful tool in indicating the properties at an amicroscopic level and is regarded as necessary complements in explaining the capturing process shown in Figure 1. In order to verify the possibility of the molecular recognizing mechanism model, a molecular geometric optimization for the host-guest system by using Gaussian 16 package is performed, where the B3LYP exchange-correlation functional and a basis set of 6-31g(d) for H, C, N, S and Lanl2dz for Cu are used. In this calculation, the surrounding water solvent is considered by the widely used polarizable continuum model (PCM). It would be relatively time-consuming for the host-guest system to spontaneously form a complex from a completely disordered initial state that has been used in many simulation calculation [23], a pre-setup where Cu^{+} is close to the middle N atom of Probe X was applied. However, to our surprise, instead of continuing to complex with N atom, Cu^{+} spontaneously approached to the S atoms and form stable coordinate bonds as shown in the video. The final result of the configuration was shown in Figure 2H.

2.7 Drug formulation and characterizations

The classic emulsion-solvent evaporation method was used to prepare the micelles used in this project. Briefly, the mixed solid with all compositions (Probe X, DOX and polymers, 10 mg) was dissolved in methanol (5 mL) to form a transparent solution, then methanol was totally removed under vacuum to yield a membrane on the inside wall. Afterwards, deionized water (10 mL) was slowly injected into the flask and sonicated for 0.5 h at room temperature to obtain the micellar solution with obvious opalescence. All micelles were freshly prepared for DLS/TEM characterizations and antitumor efficacy. The TEM samples were obtained by dripping the micellar solution to a copper TEM net, followed by complete drying under an infrared lamp.

HPLC was used to evaluate the loading content (LC) and encapsulation efficiency (EE) of micelles. ACN (1 mL) was added to collapse the assembly of drug-loading micelle (0.1 mL), 20 μL of which was submitted to HPLC for determination. The HPLC condition for Probe X: InertSustain® C18 column (5um, 4.6×250 mm); Column temperature: 25 ^{o}C; flowing rate: 1 mL/min; detector: VWD (UV-vis): 214 nm; gradient flowing phase: 0~18 min, 60% to 30% ACN in water, 18~18.5 min, 30% to 60% ACN in water, 18.5~20 min, 60% back to 30% ACN in water. The HPLC condition for DOX is: Agilent ODS C18 column (4.6×250 mm, 5 μm particle size); flowing phase: KH_2PO_4 (10 mM, aqueous):ACN:acetic acid=70:30:0.3 (v:v:v); flowing rate: 1.0 mL/min; column temperature: 25 ^{o}C; detector: fluorescence detector λex/em = 480/560 nm.

LC and EE of Probe X or DOX were calculated according to the following formulas.

LC (%) = (the mass of loaded drug/the total mass of whole micellar materials)×100%.

EE (%) = (the mass of loaded drug/the total mass of fed drug)×100%.

2.8 Confocal imaging of cellular uptake

MDA-MB-231 cells were incubated in DMEM supplemented with 10% FBS plus 1% (v:v) antibiotic. MDA-MB-231 cells were seeded with a density of 2×10^4 per well in 24-well plates (Corning, Shanghai, China), and cultured at 37 ^{o}C and 4% CO_2 for 48 h until an 80–90% confluency. The cells were incubated with glucose-free DMEM medium for 12 h to achieve a balance. The cells were then cultured with targeting CPLP-X micelles (constructed with 20% CPLP and 80% PLP, based on our previous research) for 15~60 min. Then, the cells were washed thrice with glucose-free Hank's solution, monitored by fluorescence microscopy (Leica, Wetzlar, Germany).

2.9 *In vivo* distribution observed by IVIS imaging

The formulations of free X, free IR780, PLP-X, CPLP-X and CPLP-IR780 were

firstly prepared and injected into tumor-bearing mice (X: 5mg/kg body weight) *via* the tail vein, where IR780 plays as the "Always-ON" reagent. The *in vivo* imaging of tumor-bearing mice post i.v. injection over time with different formulations were observed by IVIS. The *ex vivo* images by IVIS (PerkinElmer, Waltham, USA) of excised main organs isolated from tumor-bearing mice observed 12 h post injection with different formulations

2.10 Cell viability and *in vitro* antitumor efficacy

The *in vitro* cytotoxicity of Probe X and DOX on HEK-293 and MD-MBA-293 were evaluated using the MTT assay. Briefly, the cells were seeded into 96-well plates and then incubated separately with Probe X or DOX with various concentrations for 48 h. The MTT reagent was added to each well and further incubated for 0.5 h. Then, the medium was removed and 200 μL of DMSO was then added to each well. After shaking for 0.5 h at room temperature at dark, the absorbance of each well at 490 nm was measured with a microplate reader (BioTek Epoch, Winooski, VT, USA).

2.11 *In vivo* antitumor efficacy

All animal experiments and benefits were strictly complied with Institutional Animal Care and Use Committee of School of Pharmacy Fudan University. Female balb/c nude mice of 6 weeks with about 20 g body weight were from Department of Experimental Animals of School of Pharmacy Fudan University, and cultured under requested aseptic conditions. 1.5×10^6 MDA-MB-231 cells in 120 μL of Matrigel (5 mg/mL, BD Biosciences, Bedford, MA, USA) in PBS 7.4 were injected into the second right mammary fat-pad of nude mice to establish the tumor-bearing mice. Two weeks post the injection, the mice were randomly divided into 6 groups (n=6). The tumor-bearing mice were intravenously administrated with the formulations of saline, free X, free DOX, PLP-DOX/X, CPLP-X, CPLP-DOX, and CPLP-DOX/X at an equivalent DOX dosage of 5 mg/kg and X dosage of 5 mg/kg body weight (7 days×3). The tumor size and body weight of the mice were recorded every 3 days. The tumor volume was measured with a vernier caliper and calculated with the formula: tumor

volume=(lump length)×(lump width)^2/2. All mice were sacrificed on the 30th day. The tumors and main organs were carefully excised and rinsed with PBS 7.4 for further photographs. TUNEL assay was carried on 5 μm frozen tumor slices using a DNA fragmentation detection kit according to the regular protocols provided by the producer and observed by fluorescent microscope (Leica, Wetzlar, Germany).

2.12 Photoacoustic imaging

The animal and phantom tests were performed by a multispectral Photoacoustics Imaging System (Visusal Sonics, Vevo LAZR, Toronto, Canada). For the *in vivo* photoacoustic imaging of the tumors, the mice were i.v. injected with different formulations 24 h before the imaging (λex=730 nm). To monitor the tumor's modulated oxygen saturation, the mice experienced a 3-round treatment with different formulations.

2.13 *In vitro* tube-formation and wound-healing

Probe X (25 μg/mL) was mixed with Matrigel matrix (BD Biosciences, MA, USA) and added to the 48-well plates, which were placed at 37 ^{o}C for 1 h to solidify. Then, human umbilical vein endothelial cells (HUVECs) in 200 μL basic DMEM containing 2×10^5 cells were seeded onto these matrices and further incubated for 12 h. Then, random fields in each well were observed at different intervals under a microscope (Olympus, Tokyo, Japan).

HUVECs were seeded into the 6-well plates at a density of 10^5 cells/well and incubated for 48 h to form a monolayer. Then, a single linear wound to the layer was caused with a pipette tip carefully, further incubated with Probe X (25 μg/mL) in basic DMEM for 24 h. Defined wound line at fixed part in each well was observed at different intervals under a microscope (Olympus, Tokyo, Japan).

2.14 Cu determination by ICP-Ms

The tumors randomly selected from four mice each group were homogenized and then digested in 70% nitric acid at 80 °C for 24 h until no solid tissues were left. The

suspension was dispersed in ultrapure water and the copper contents in all samples were detected using ICP-Ms.

2.15 Histochemistry analysis

The main organs were excised, fixed with 4% paraf-ormaldehyde solution (v/v in water) for 12 h, followed by being frozen in the OCT embedding medium (Sakura, Torrance, CA, USA) at -80 ^{o}C. Pictures of the stained slices were photographed under the inverted fluorescent microscope (Leica, Wetzlar, Germany) for histochemistry analysis.

2.16 Data analysis and statistics

All the data were presented as means ± SD, and comparison between groups was performed by GraphPad Prism. Statistical significance was defined as $p < 0.05$.

3. Results and discussion

3.1 Design, theoretical calculation and synthesis

We first started the project by selecting a specific chelating ligand, as well as a tracker, for Cu^{+} both *in vitro* and *in vivo*. With the aim of facially capturing metal ions, various types of ligands have been developed and widely applied in MRI and biomedical sciences, to name a few, 1,4,7,10-tetraazacyclododecane-1,4,7,10-tetraacetic acid (DOTA), 1,4,7-triazacyclononane-1,4,7-triacetic acid (NOTA) [24] and tetrathiomolybdate (TM) [25]. Most of the developed chelating ligands, however, have limited selectivity to metal ions, which will easily result an unexpected loss of entogenous essential metals once applied. It is with great realistic meaning in finding a specific chelating ligand for Cu^{+}. Different from Cu^{2+} chelators, Cu^{+} strongly prefers ligands with softer donor atoms such as thioether S and aromatic N [26].

On the other hand, human body is a “black box” to scientists, and upon the substrates delivered into the body, the information of “where/when/how/how much” of the distribution and spatio-temporal accumulation is difficult to be monitored in a real-time way. Tissue extraction method can definitely provide useful messages,

which, however, is time-consuming, hysteretic and traumatogenic. Since Cu is an essential element for life, while alterations in its cellular homeostasis other than tumors are connected to serious diseases or side effects, including leukoderma, Menkes and Wilson diseases by undiscriminatingly capturing Cu from the Cu-relying enzymes [27–28]. In this regard, real-time reporting the Cu-caging phenomenon in a theranostic strategy, especially upon *in vivo* situation, can provide rich information on drug tracking, efficacy prediction and clinical guidance with lowered side-effect. However, developing reliable optical imaging ligands with Cu^+-selective fluorescent sensors is still facing tremendous challenge, since Cu is normally used as a fluorescent-quenching reagent. Indeed, instead of the "OFF-to-ON" type, we initially did plan to create an "ON-to-OFF" type fluorescent sensor upon the recognition of the ligand to Cu^+. However, the fluorescence quenching can be attributed to various unpredictable reasons (photobleaching, solvent effect, aggregation caused quenching, etc), besides Cu^+ capture. After attempts, we finally successfully obtained an "OFF-to-ON" type NIR fluorescent sensor (Probe X) derived from IR780. Probe X can be used as a Cu^+ tracker, as well as a Cu^+ chelator. The synthesis steps of the chelators (compound 2 and Probe X) were shown in Figure 1.

In order to realize the targeting delivery of the ligands and chemotherapeutic, through a ring-opening reaction initiated by PEG-NH_2, we also developed a bio-friendly polypeptide-based amphiphile (PLP, Figure 1), which can load the hydrophobic substrates and self-assemble into micelles in the aqueous solution. The cyclic peptide cRGD, that is proved capable to target the tumors' newborn vessels, was anchored to the polymer to obtain CPLP. Through the active (cRGD) and passive (EPR effect) targeting, the micelles are hopefully able to reach the aimed sites effectively.

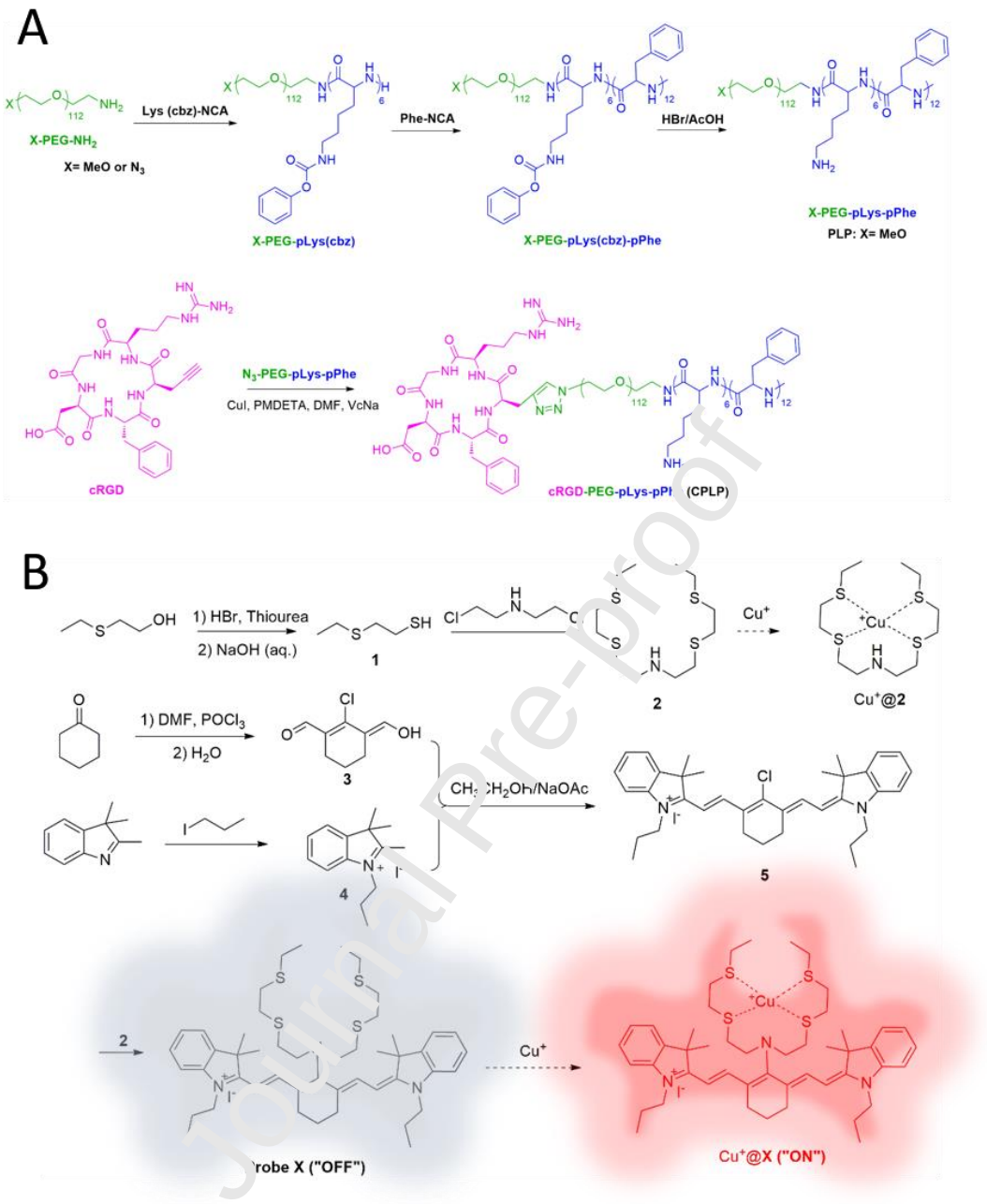

Figure 1. Synthesis of (A) the amphiphilic polypeptides (CPLP and PLP, blue: hydrophobic; green: hydrophilic; purple: cRGD) and (B) Cu^{+} chelator (Probe X, gray: OFF state; red: ON state).

3.2 Molecular recognition between Probe X and Cu^{+}

We then investigated the specific Cu^{+} capturing capability of Probe X in aqueous solutions by multiple means. In presence of increasing amount of Cu^{+}, the intensity of excitation spectrum of Probe X tended to be stronger (Figure 2A), which suggests the

addition of Cu^+ can help Probe X gain more energy from the irradiating photons. On the other hand, the emission is found simultaneously increasing (Figure 2B). In absence of Cu^+, the fluorescence is relatively weak, while the Probe X/Cu^+ complex can give much stronger fluorescence. The UV-vis spectra of sole X and X+Cu^+ were also undertaken, where a clear red-shift was noticed for X+Cu^+ (Figure S11). This indicated the formation of a new species, which performed a stronger absorbance at the excitation wavelength of fluorescence. The combined results suggest an "OFF-to-ON" ability of Probe X to detect/complex Cu^+, where the mechanism could be an increased energy-gaining capability for the fluorescence, since fluorescence is essentially an energy-transfer phenomenon.

Then we employed the classic Job's continuous variation method to determine the complex stoichiometry of Probe X/Cu^+, where the maximum value was found at a molar ratio (Probe X/(Probe X+Cu^+)) of 0.5. This signified that Probe X/Cu^+ tended to stay in a 1:1 stoichiometry mode. We then explored the selectivity of Probe X to different cations that are common *in vivo*. It was noticed that only Cu^+ can induce strong fluorescence. When facing cations other than Cu^+, Probe X is still in an "OFF" state, while upon addition with Cu^+ to the above solutions, strong fluorescence can be recovered. FT-IR can be used in studying the supramolecular interactions between ligands and metal ions. The FT-IR spectra of Probe X, Cu^+, the corresponding physical mixture and complex of X/Cu^+ in KBr were undertaken. The physical mixture and complex of X/Cu^+ have the exactly same chemical composition, however, they gave greatly distinctive results. The spectrum of physical mixture is clearly the overlying of the spectra of starting materials (X/Cu^+), for example, the peaks at the wavelength at 2937 and 831 cm^{-1}. Meanwhile, new peaks can be recognized at the spectrum of the complex, revealing the complex is a new species and new interactions were formed between X/Cu^+.

We then employed geometric optimization to mimic the recognition procedure (Figure 2G and supporting video). Cu^+ was released to the system in a free state, and after a relatively long balancing, Cu^+ automatically approached the ligand area to form a stable complex. Meanwhile, the original configuration of Probe X was slightly

perturbated, especially observed from the lateral view. Both ligands were attached to the molecule *via* rotatable covalent bonds, allowing Probe X with appropriate configuration to hunt Cu^+ in the solvent. From the vedio of the detailed molecular recognition process, Cu^+ firstly attached with the middle N atom of Probe X temporarily. After short interactions with N atom, Cu^+ more tended to be attracted by the S-containing ligands, and both ligands became curved and curled to cage Cu^+ in the middle to form a stable complex. Upon completion the molecular recognition, the systematic energy slightly rises 0.07 eV based on the calculation, which is easily overcome from the environment disturb. The Off-to-ON procedure mechanism could be: the electron rich S atoms (also Cu^+ receptor) are able to quench the fluorescence of the tricarbocyanine backbone, and upon capturing with Cu^+, the quenching influence is inhibited to further recover the fluorescence.

Then the Cu^+ recognizing capability of Probe X was evaluated on MD-MBA-231 (human triple negative breast cancer cells) and HEK-293 (human embryonic kidney) cells. Since endogenous Cu^+ is much richer in tumor cells than somatic cells, the fluorescence intensity is much stronger on MD-MBA-231 than HEK-293 (Figure 2I) in accordance with the cell types. Introduction with exogenous Cu^+ can increase, and extra Cu^+ chelator (compound 2) can decrease the fluorescence intensity of both cells. The fluorescence intensity of tumor cells was also found obviously increased upon introduction with Vitamin C (VC) that can trigger the release of labile endogenous Cu^+ in living cells [29]. The results were further verified using flow cytometry, where a large number of cells with "Turned-ON" fluorescence emission was found upon treated with sole Probe X (1 mM). At this concentration of Probe X, introduction with exogenous Cu^+ cannot increase the number of "Turned-ON" cells, suggesting the buffered Cu^+-capturing ability of 1 mM Probe X and endogenous Cu^+ can already satisfy the chelating of Probe X. We further carried on the same experiments on HEK-293 cells, and found exogenous Cu^+ can give an apparent rise to the number of "Turned-ON" cells, since exogenous Cu^+ in HEK-293 cells is initially at a low level. Taken together, the combined results suggest tumor cells contain much more Cu^+ than body cells. Probe X can be employed in tracking/capturing endogenously produced

Cu^{+}, no matter in buffers or physiological medium.

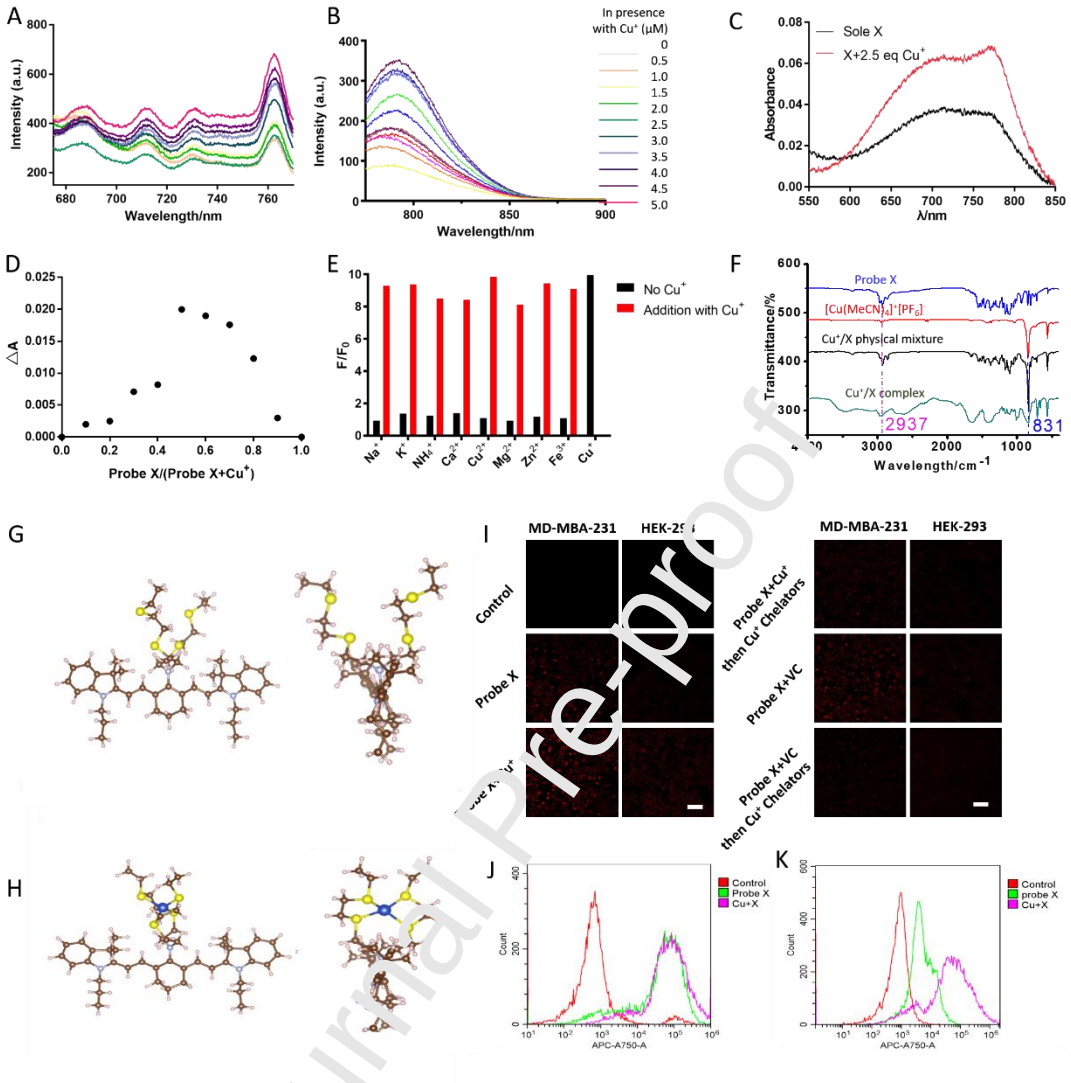

Figure 2. (A) The excitation and (B) the emission spectra of Probe X in presence with different Cu^{+} concentration in mixed methanol/water (2.5 mM, v:v, 1:1), λex/em=750/792 nm; (C) the red-shift of the UV-vis absorbance of Probe X in presence of Cu^{+} in mixed methanol/water (v:v, 1:1); (D) The complex stoichiometry of Probe X/Cu^{+} determined by Job's continuous variation method using a UV-vis spectrometer; (E) fluorescence responses of the Probe X (2.5 mM) to various cations in the aqueous buffer (pH 7.0, 25 mM PBS buffer with 10% ethanol, 2.5 mM), where the black bars represent the addition of an excess of cations (2.5 mM) to a solution of Probe X, and red bars represent the subsequent addition of 2.5 mM Cu^{+} to the above solutions (λex/em=750/792 nm); (F) the comparision of the FT-IR spectra of Probe X, Cu+, physical mixture and complex of X/Cu^{+} in KBr; (G) the Probe X's molecular

configuration variation before and after the Cu^+ capture; (H) fluorescence images of MD-MBA-231 and HEK-293 cells treated with different formulations (**control**: no treatment; **Probe X** (5 μM); **Probe X+Cu$^+$**: pretreated with $CuCl_2$ (200 mM, Cu^{2+} can be rapidly transformed into Cu^+ in the cells in presence of GSH) for 7 h and further incubated with Probe X (5 mM) for 10 min at 37 ^oC; **Probe X+Cu$^+$ then Cu$^+$ chelators**: pretreated with $CuCl_2$ (200 mM) for 7 h, further incubated with Probe X (5 mM) for 10 min at 37 ^oC, and subsequently treated with a competing Cu^+ chelator compound 2 (50 μM) for an additional 10 min at 37 ^oC; **Probe X+VC**: pretreated with VC (1 mM) for 4 h and then incubated with Probe X (5 mM) for 10 min at 37 ^oC; **Probe X+VC then Cu$^+$ chelators**: pretreated with VC (1 mM) for 4 h, further incubated with Probe X (5 mM) for 10 min at 37 ^oC, and subsequently treated with a competing Cu^+ chelator compound 2 (50 μM) for an additional 10 min at 37 ^oC); (I) the quantitative determination of MDA-MB-231 cells with NIR fluorescence using flow cytometry (**Probe X** (5 μM, 10 min); **Probe X+Cu$^+$**: pretreated with $CuCl_2$ (200 mM) for 7 h and further incubated with Probe X (5 mM) for 10 min at 37 ^oC) with scale bars=25 μm; the quantitative determination of (J) MD-MBA-231 and (K) HEK-293 cells with recovered fluorescence using flow cytometry (**Probe X** (5 μM, 10 min); **Probe X+Cu$^+$**: pretreated with $CuCl_2$ (200 mM) for 7 h and further incubated with Probe X (5 mM) for 10 min at 37 ^oC).

3.3 Drug formulation

Both the selected cytotoxic drug (DOX) and Probe X possess conjugated systems, we decided to employ PEG-*p*Lys-*p*Phe (PLP) as the building block to construct the nanomicelle, where poly-phenylalanine plays as the hydrophobic part of the amphiphile. The *p*Phe part will self-assemble into hydrophobic core to encapsulate DOX and Probe X *via* hydrophobic interactions, and more important, π-π stacking effect, with the aim to form a micelle with high drug loading rate and stability.

The preparation of the micelles loading with DOX/X was optimized, and the PLP-DOX/X and CPLP-DOX/X micelles (the formulation with active-targeting ability, doped with 20% cRGD-PLP composition, based on our previous research [30])

in PBS 7.4 were obtained. The micellar solutions were dried under vacuum and observed under TEM, where spherical micelles with uniform morphology ranging from 20 to 60 nm were found for both micelles (Figure 3A and B). The PLP-DOX/X and CPLP-DOX/X micellar aqueous solution is homogeneous with opalescence, and typical Tyndall effect can be found, while obvious solid can be found if DOX/X in DMSO was directly dispersed in PBS 7.4. The size distribution was further verified using dynamic light scattering (DLS, 56.1±5.2 nm for PLP-DOX/X and 62.7±3.4 nm for CPLP-DOX/X) and nanoparticle tracking analysis (NTA). No aggregates smaller than 10 nm were tested, meaning a fine dispersion and encapsulation. It is understandable the diameters measured by DLS were slightly larger than TEM, since DLS data are from the hydrodynamic diameters, while TEM is measuring the solid spheres [31]. We also found an increase of the Z potential before and after the encapsulation (Figure 3F), which could be ascribed to the loaded DOX and X with potential positive charges. After optimization, the drug loading rate and encapsulation efficiency are measured to be 19.3% and 89.7% by HPLC, respectively (DOX:X=1:1, w:w).

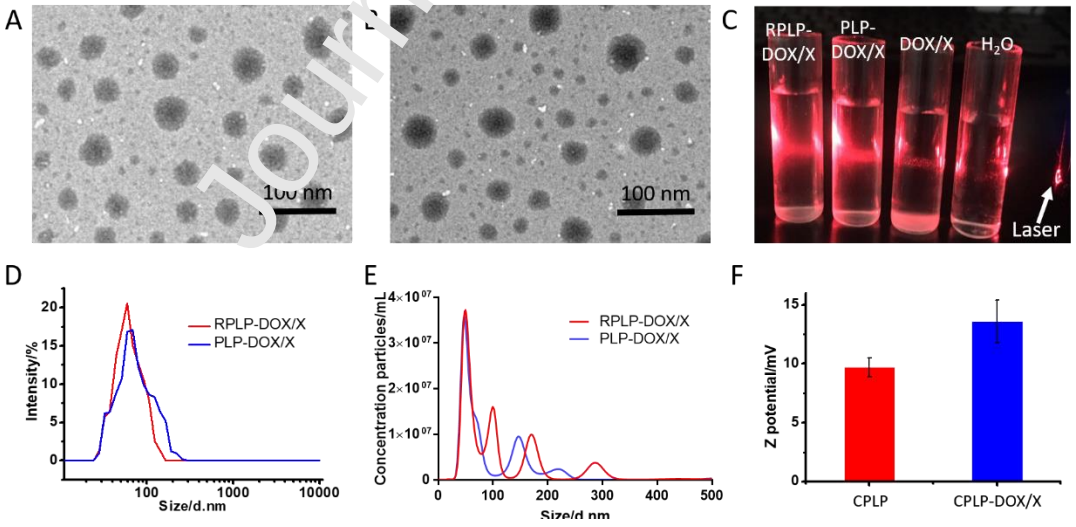

Figure 3. TEM images of (A) PLP-DOX/X and (B) CPLP-DOX/X micelles; (C) Tyndall effect of PLP-DOX/X and CPLP-DOX/X micelles in PBS 7.4; size distribution of PLP-DOX/X and CPLP-DOX/X micelles in PBS 7.4 measured by (D) DLS and (E) NTA; (F) Z potentials of PLP-DOX/X and CPLP-DOX/X micelles in

PBS 7.4.

3.3 Drug distribution

CPLP-X micelle ("OFF" state) was used to treat MD-MBA-231 cells and monitored under confocal imaging system to study the cellular internalization pathway and reveal the detailed "OFF-to-ON" process (Figure 4A). When incubated for 15 min with CPLP-X micelle, clear nanoparticles with fluorescence ("ON" state) were observed and co-localized with lysosomes. The nanoparticles still stayed in an orbicular state, meaning the fluorescence of Probe X molecules were still encapsulated in the micellar core but already triggered ON. On the other hand, Cu^+ is relatively rich in tumor cells and can be rapidly absorbed into the micellar core, though normally regarded hydrophobic. Upon 60 min, a lysosome-escape and extensive fluorescence in cytoplasm were found. In this procedure, Probe X that is still available was dissociated into the cytoplasm to capture residual Cu^+ in the cell. In combination, an apparent internalization transfer *via* lysosomes into cytoplasm, accompanied with the "OFF-to-ON" procedure was revealed.

Photoacoustic imaging is a noninvasive technique with high imaging depth (ca. 10 cm) that can provide higher optical resolution at depths inaccessible by other optical approaches [32]. It was reported that Cu can strengthen the photoacoustic imaging capability of heptamethine cyanine dye [33]. We further used the Probe X-loading micelles as photoacoustic imaging reagents. The targeting CPLP-X micelle can give the strongest photoacoustic signal at the tumor sites in all tested four groups (Figure 4B and C), which should be due to the highest tumor accumulation of CPLP-X from both passive (EPR effect) and active targeting (cRGD) effect.

Encouraged by these results, we further investigated the drug distribution and "OFF-to-ON" procedures *in vivo* by IVIS (Figure 4E). Formulations of free Probe X (OFF), free IR780 (already-ON), PLP-X, CPLP-X and CPLP-IR780 with the same molar amount of the dyes were injected into the tumor-bearing mice *via* tail vein. No obvious signal can be detected in Probe X group at 2 h, which could be explained by the uncontrollable distribution and the relatively low concentration of Cu^+ *in vivo*. It is

possible that Probe X mostly distributed in a specific organ, but it showed low florescence due to the low concentration of Cu^+. Surprisingly, even without specific formulation, clear NIR fluorescence signal could be monitored only at the tumor sites, which tended to be even stronger as time extended until 24 h. This further verified the higher concentration of Cu^+ in tumors that is essential in expanding new vessels. As to the IR780 group, since fluorescence signal is always-ON, we noticed strong fluorescence signal systemically that vanished over time possibly due to the metabolism and excretion. At 24 h, only residual signal can be found at the tumor sites. It is understandable since the dyes of indocyanine green family have been approved by FDA in clinical angiography [34]. Noteworthy, evident liver metabolism of PLP-X was observed at 2 h. However, due to the EFR effect, the tumor accumulation predominated. On the other hand, tumor accumulation of CPLP-X is stronger, suggesting the important role of the active targeting inherited from cRGD. No severe liver accumulation but a kidney excretion was noticed. The NIR signal elevation in the tumors is from the increasing accumulation, as well as the "OFF-to-ON" procedure of Probe X capturing the *in situ* Cu^+. As the control, the NIR signal at the tumor site is always strong for the CPLP-IR780 group that is already ON. The results were further verified by the *ex vivo* images of excised main organs isolated from tumor-bearing mice observed 12 h post injection with different formulations. Limited signal was monitored in the liver. We deduce the NIR light has limited penetration capability, which makes IVIS more suitable in monitoring drug distribution in relatively superficial tumor [35], such as breast cancer. On the other hand, liver is located deep in cavum abdominis, which is sometimes difficulty and direct to be observed by IVIS, though useful information can be obtained in a tempo-way. The spatio-information is more reliable if we try to investigate the distribution *ex vivo* on the isolated organs (Figure 4D), where the liver accumulation is obviously unneglectable. In combination, CPLP micelle can target and accumulate into the tumor to result an "OFF-to-ON" NIR signal. The real-time activatable theranostic phenomenon is of potential application in clinic [36].

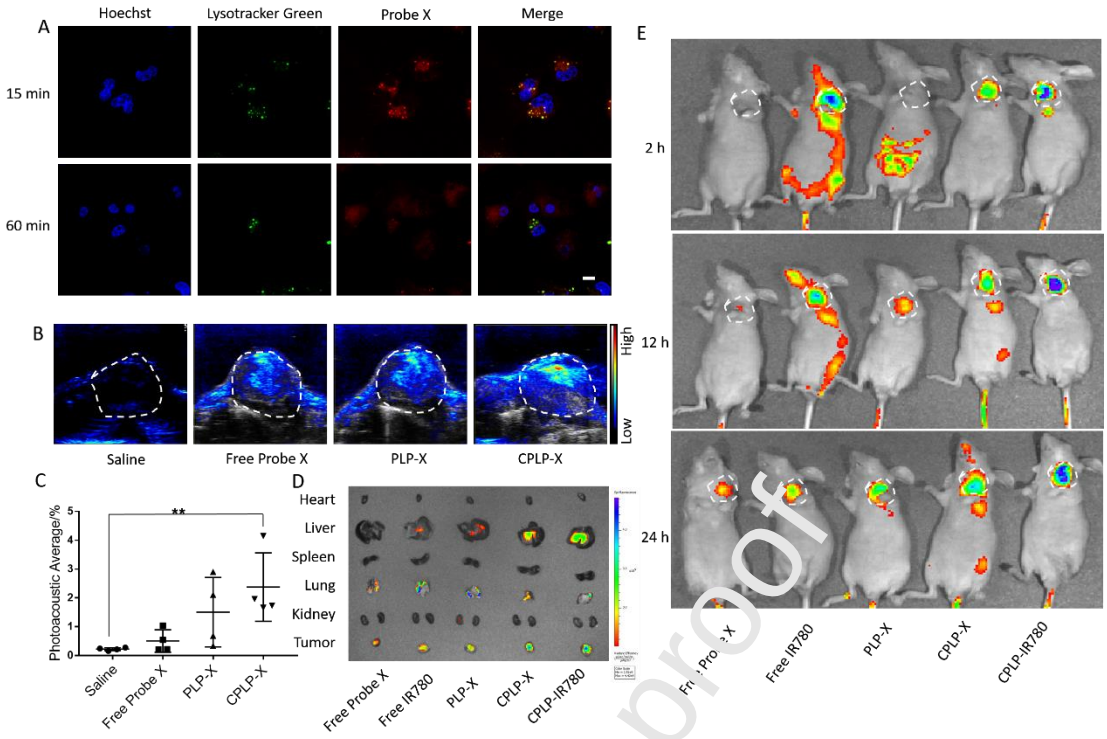

Figure 4. (A) Confocal imaging of cellular uptake of the targeting CPLP-X micelles after incubation for 15 and 60 min on MDA-MB-231 cells with scale bar=5 μm; (B) *in vivo* photoacoustic imaging of the tumors in white circle 24 h post i.v. injection with different formulations; (C) semi-quantitation of the *in vivo* photoacoustic imaging (λex=730 nm) of the tumors in white circle 24 h post i.v. injection with different formulations (n=4), (D) *ex vivo* images by IVIS of excised main organs isolated from tumor-bearing mice observed 12 h post injection with different formulations; (E) *in vivo* imaging of tumor-bearing mice post i.v. injection over time with different formulations observed by IVIS, where the white circles represent tumor positions.

3.4 Antitumor efficacy

With above data in hand, the antitumor efficacy of the proposed strategy was further evaluated. Cu^{+} is not just impotent in building new vessels in the tumor, but also in serving as an essential catalytic cofactor for enzymes that function in antioxidant defense, iron homeostasis and cellular respiration [37]. Down-regulating the intracellular Cu^{+} concentration and trafficking of Cu^{+} in the cells provides a promising route to enhance the cytotoxicity of chemotherapeutic agents by disrupting

these above processes. It was found the IC_{50} concentration of DOX can decrease 52 times (from 8.649 to 0.1623 μg/mL) when co-treated with Probe X (Figure 5A and S12). The applied concentration of Probe X is 6 pmol/L, at which concentration, the cell viability (just Probe X) can still reach over 80%. At nearly all concentrations, Probe X can enhance the antitumor efficacy of DOX. This suggests a fine synergistic effect of DOX and Probe X in the anti-tumor applications. Motivated by this, we then carried out the *in vivo* antitumor efficacy test. The tumor-bearing mice were intravenously administrated with the formulations of saline, free X, free DOX, PLP-DOX/X, CPLP-X, CPLP-DOX, and CPLP-DOX/X at an equivalent DOX dosage of 5 mg/kg body weight every (7 days×3). The tumor size and body weight of the mice were recorded every 3 days. Among all groups, CPLP-DOX/X shows the most evident suppression effect on tumor growth (Figure 5B~D). In addition, the body-weight of all groups was rather stable with regular fluctuations, suggesting minimized systemic toxicity (Figure 5E). During the treatment, the body weight decreased apparently upon treated with free Probe X and DOX, suggesting the unneglectable systematic toxicity.

After 3-round therapy, the tumors were excised from the sacrificed mice in all groups to investigate the neoangiogenesis. Triple negative breast cancer (TNBC), used as the model in this study, is a typical type of tumor marked with adequate blood perfusion, and neoangiogenesis is crucial in the cancer progression [38]. Trafficking Cu^{+} could be of great beneficence in attenuating the proliferation and motility of endothelial cells in tumors [39]. CPLP-DOX/X demonstrated the most significant effect in decreasing neoangiogenesis (Figure 5F). On the other hand, formulations only containing DOX show little efficacy in decreasing neoangiogenesis. The combined results verified a favorable synergistic effect of DOX and Probe X in anti-tumor applications by means of cytotoxic effect and decreasing neoangiogenesis simultaneously.

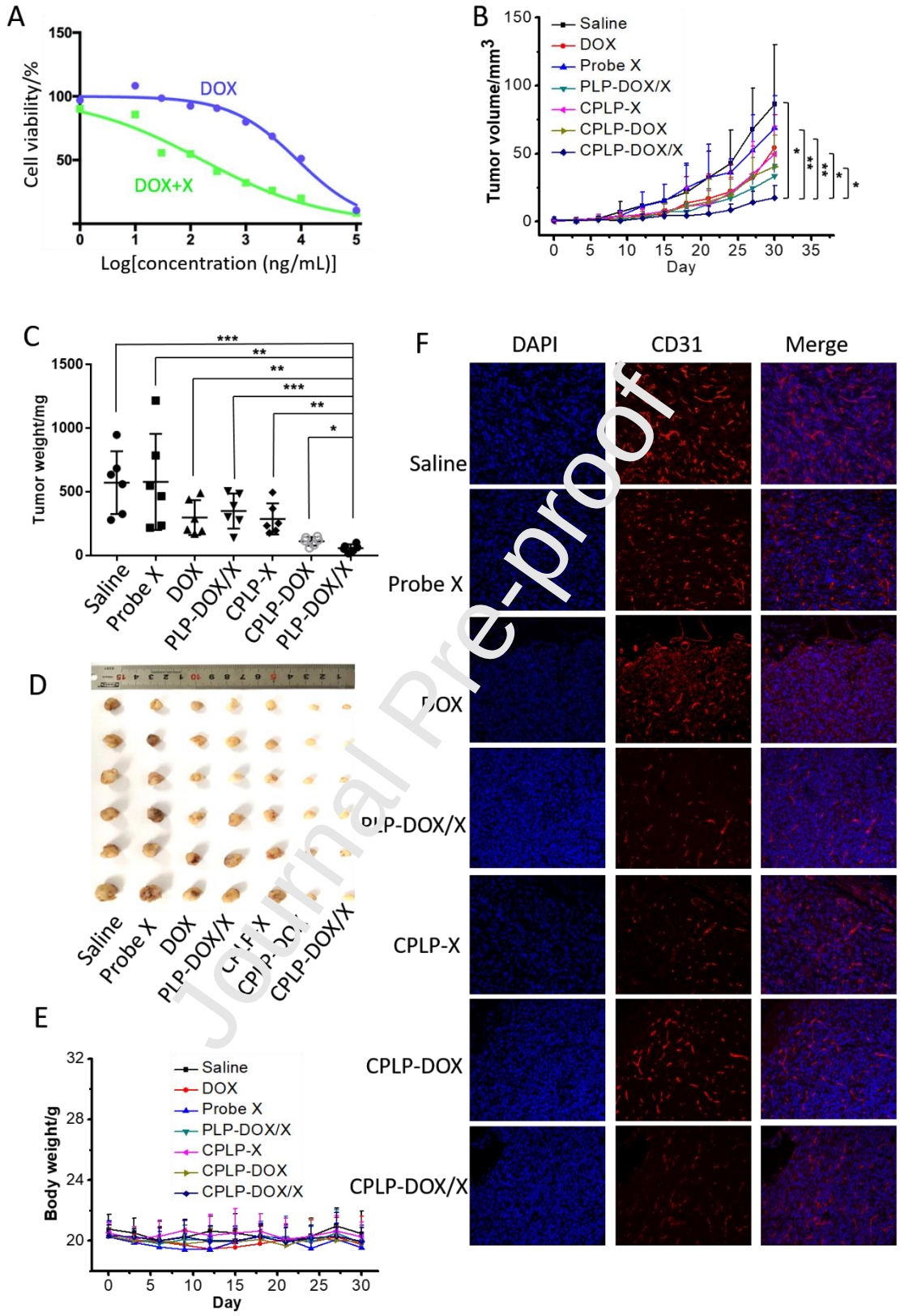

Figure 5. (A) *In vitro* cell viability to MD-MBA-231 cells of DOX in absence and presence (Probe X is set constant at 6 pmol/L.) of X evaluated by MTT assay; *in vivo* antitumor efficacy study of tumor volume (B), excised tumor weight (C), tumor

images (D) and body weight (E), where data were recorded every three days during 30 days treatment course (n = 6, *P < 0.1, **P < 0.01 and ***P < 0.001); (F) *in situ* TUNNEL staining of breast tumors from mice 30 days treatment course with all formulations, where nucleus of tumor cells (DAPI, blue) and tumor-related new vasculature (CD31, red) were labeled (×400).

3.5 Mechanism study

Based on the *in vivo* antitumor efficacy findings, the mechanism was further investigated. From Figure 5F, the *in vivo* neoangiogenesis was greatly decreased after targeted delivery with Cu^+ ligand. Inspired by this, we studied the mechanism by undertaking the *in vitro* antiangiogenic effects. HUVECs can uptake Cu in the serum to induce the angiogenesis mimesis during the incubation as shown in Figure 6A. Meanwhile, the migration of HUVECs could be also found by means of the wound healing assays (Figure 6B). Upon treated with Probe X as the Cu^+ removal reagent, the cells tended to be rounded, while the wound-healing was distinctly inhibited. Notably, Cu-deficiency strategy can also inhibit the cell proliferation from Figure 6B. The *in vivo* tumor's oxygen saturation after a 3-round treatment was also evaluated by photoacoustic imaging (Figure 6C), where the CPLP-X group show ca. 21% oxygen saturation in comparison with the control group.

Cu concentration *in vivo* is strongly related with the types of cell, tissue or organ, because excess Cu ions are harmful to the body. Cu plays an important part in the development and invasion of tumors and normally reaches higher level than other parts of the body. The concrete Cu concentration in tumors of all groups was also quantified by ICP-Ms (Figure 6D), where the Cu concentration in CPLP-X group is only ca. 11% in comparison with the control group. Considering the fact of antineoangiogenesis shown in Figure 5F, the combined results suggest the mechanism could be: efficient caging Cu^+ can cause substantially negative influence to the motility of HUVECs, obviously decrease O_2-saturation in the tumors, and finally inhibit the growth. Though it is still contestable whether the Cu-deficiency in tumors could be buffered with the substance exchange somehow, however, the Cu-deficiency

induced the lack of neovascularization will result a vicious spiral and nutrients (including Cu) required by tumor progression will be limited. Under this consideration, Cu concentration can be regarded as the biomarker in discriminating the tumor and normal tissues, as well as indicating the Cu deficiency progress, to realize the theranostics effect.

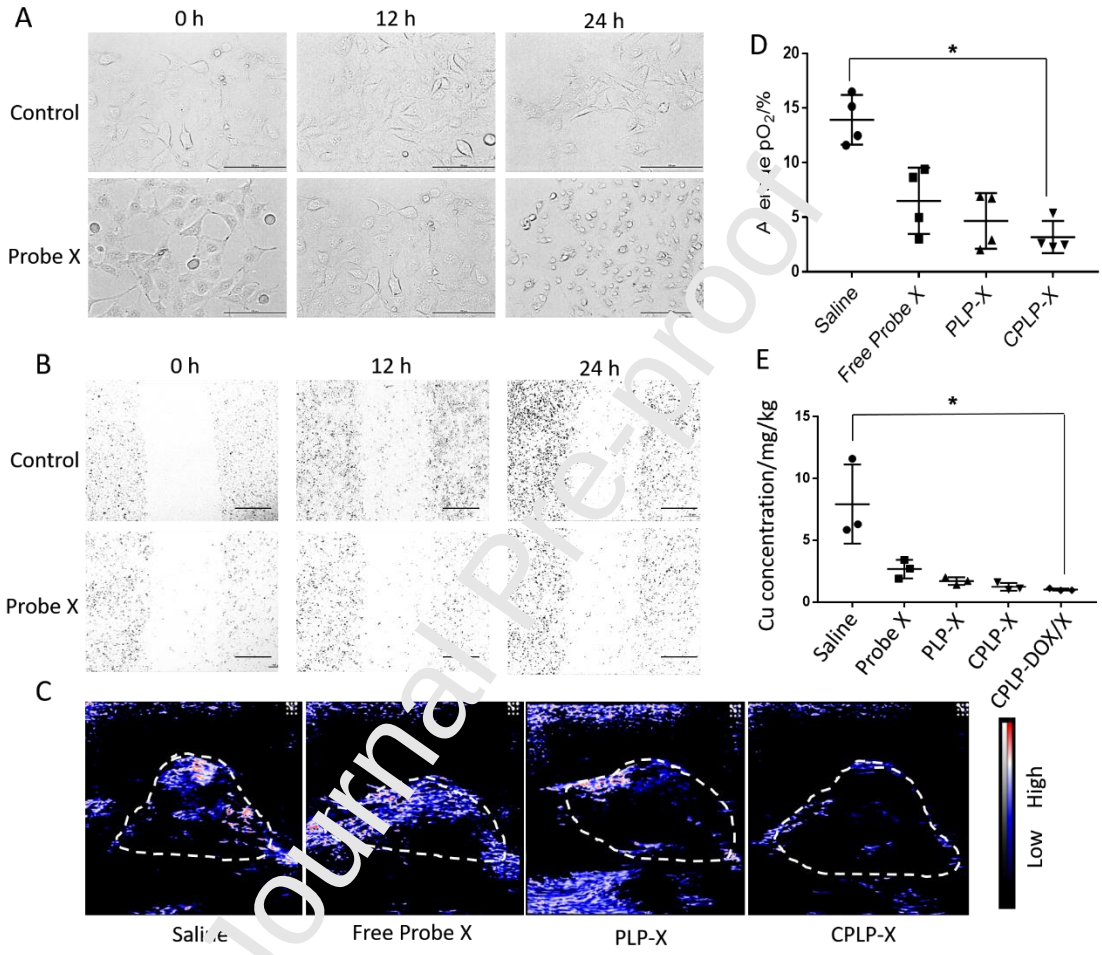

Figure 6. The tube-formation (A, scale bars=150 μm) and wound-healing (B, scale bars=0.5 mm) abilities of HUVECs treated with Probe X; (C) the tumor's oxygen saturation after a 3-round treatment with different formulations evaluated by photoacoustic imaging; (D) semi-quantitation of the *in vivo* oxygen saturation of the tumors by photoacoustic imaging after a 3-round treatment with different formulations (n = 4, *P < 0.1); (E) Cu concentration in tumors determined by ICP-Ms (n = 3, *P < 0.1).

3.6 Toxicity evaluation

It was reported that systematic injection with Cu chelator can lead to severe side effect as discussed in the introduction part, which could be due to the unexpected chelator distribution and nondiscriminating Cu exclusion from the body, since Cu is an essential element [40]. Thus, tumor-targeting delivery with Cu chelator proposed in this study, which could hopefully realize a specific elimination, is necessary in reducing the side effect and of great potential applications in clinic [41]. The *in vitro* cytotoxicity to HEK 293 and MD-MBA-231 cells of Probe X was evaluated by MTT assay (Figure 7A and B), where Probe X show much stronger cytotoxicity to MD-MBA-231 than HEK 293 cells. Cu levels are often elevated in tumor cells, and the Cu^{+}/Cu^{2+} pair is playing a more important role in tumor cells in balancing the ROS level [42]. Removal Cu from tumor cells is more fatal than somatic cells.

Based on the histochemistry analysis shown in Figure 7C, apparent histopathological lesions of liver in the Probe X group were found (the arrow). Meanwhile, apparent abnormities in the heart of DOX group were also found (the arrow), suggesting potential cardiotoxicity. No obvious difference of solid organs was observed for other groups, suggesting a low systemic toxicity.

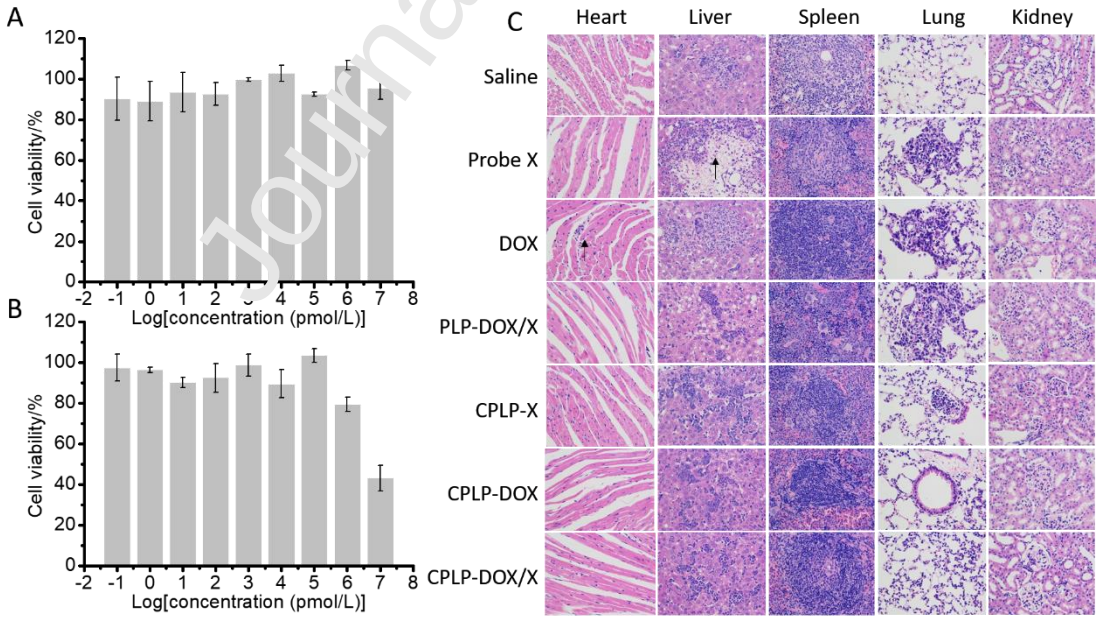

Figure 7. *In vitro* cytotoxicity to (A) HEK-293 and (B) MD-MBA-231 cells of Probe X at different concentrations evaluated by MTT assay (n = 6); (C) histochemistry analysis of heart, liver, spleen, lung and kidney sections stained with hematoxylin and

eosin.

4. Conclusion

Tumor growth and metastasis greatly rely on neoangiogenesis, where Cu^+ plays an important role [43]. In this work, we proposed a micelle system that can co-delivery of Cu^+ chelator and chemotherapeutics as a new strategy for tumor treatment strategy. Human body can be compared to a black box, and once drug was injected into the system, it is important to know the fate, though currently with much difficulty. A specific Probe X, both as the chelator and "Off-to-ON" type tracer for Cu^+, was developed. Probe X and DOX were co-loaded into a targeting micelle built from a body-friendly polypeptide amphiphile. The micelle was anchored with cRGD that can target neoangiogenesis of tumors. The micelle can target and accumulate into the tumor, to deliver DOX and Probe X, which can undergo an "OFF-to-ON" procedure upon capturing Cu^+ to give NIR fluorescence and photoacoustic signals for dual-mode real-time and non-invasive reporting the events of Cu^+-caging *in vitro* and *in vivo* ("*let there be light*") [44]. After treatment, both Cu level and oxygen saturation were significantly lowered in tumors based on which, the antitumor mechanism of anti-neoangiogenesis was studied. Finally, the *in vivo* toxicity was evaluated. The theranostic concept can serve useful in developing precision and personalized medicine for versatile clinical applications [45].

Acknowledgements

This work was supported by National Natural Science Foundation of China (81872808) and Program of Shanghai Academic Research Leader (18XD1400500), Shanghai Municipal Science and Technology Major Project (2018SHZDZX01) and ZJLab, Fudan-SIMM Joint Research Fund (FU-SIMM20182006) and Scientific Research Program of Shanghai Health and Family Planning Commission (20184Y0149).

Appendix A. Supplementary data

Supplementary data to this article can be found online at http://XXX

References

[1] C. Santini, M. Pellei, V. Gandin, M. Porchia, F. Tisato, C. Marzano, Advances in copper complexes as anticancer agents, Chem. Rev. 114 (2014) 815–862.

[2] A. Gupte, R.J. Mumper, Elevated copper and oxidative stress in cancer cells as a target for cancer treatment, Cancer Treat. Rev. 35 (1) (2009) 32–46.

[3] D. Denoyer, S. Masaldan, S. La Fontaine, M.A. Cater, Targeting copper in cancer therapy: copper that cancer, Metallomics 7 (2015) 1459–1476.

[4] H. Xie, Y.J. Kang, Role of copper in angiogenesis and its medicinal implications, Curr. Med. Chem. 16 (2009) 1304–1314.

[5] A.K. Boal, A.C. Rosenzweig, Structural biology of copper trafficking, Chem. Rev. 109 (2009) 4760–4779.

[6] H.M. Alvarez, Y. Xue, C.D. Robinson, M.A. Canalizo-Hernandez, R.G. Marvin, R.A. Kelly, A. Mondragón, J.E. Penner-Hahn, T.V. O'Halloran, Tetrathiomolybdate inhibits copper trafficking proteins through metal cluster formation, Science 327 (2010) 331–334.

[7] K. Garber, Targeting copper to treat breast cancer, Science 349 (2015) 128–129.

[8] G.J. Brewer, P. Hedera, K.J. Kluin, M. Carlson, F. Askari, R.B. Dick, J. Sitterly, J.K. Fink, Treatment of Wilson disease with ammonium tetrathiomolybdate: III. Initial therapy in a total of 55 neurologically affected patients and follow-up with zinc therapy, Arch. Neurol. 60 (2003) 379–385.

[9] T. Sun, G. Zhang, Q. Wang, Q. Chen, X. Chen, Y. Lu, L. Liu, Y. Zhang, X. He, C. Ruan, Y. Zhang, Q. Guo, C. Jiang, A targeting theranostics nanomedicine as an alternative approach for hyperthermia perfusion, Biomaterials 183 (2018) 268–279.

[10] S.C. Dodani, S.C. Leary, P.A. Cobine, D.R. Winge, C.J. Chang, A targetable fluorescent sensor reveals that copper-deficient SCO1 and SCO2 patient cells prioritize mitochondrial copper homeostasis, J. Am. Chem. Soc. 133 (2011) 8606–8616.

[11] W. Xu, Z. Zeng, J.-H. Jiang, Y.-T. Chang, L. Yuan, Discerning the chemistry in individual organelles with small-molecule fluorescent probes, Angew. Chem. Int. Ed. 55 (2016) 13658–13699.

[12] M. Taki, K. Akaok, K. Mitsui, Y. Yamamoto, A mitochondria-targeted turn-on fluorescent probe based on a rhodol platform for the detection of copper(i), Org. Biomol. Chem. 12 (2014) 4999–5005.

[13] W. Zheng, H. Li, W. Chen, J. Zhang, N. Wang, X. Guo, X. Jiang, Rapid detection of copper in biological systems using click chemistry, Small 14 (2018) 1703857.

[14] M. Khamaisi, O. Kavel, M. Rosenstock, M. Porat, M. Yuli, N. Kaiser, A. Rudich, Effect of inhibition of glutathione synthesis on insulin action: in vivo and in vitro studies using buthionine sulfoximine, Biochem. J. 349 (2000) 579–586.

[15] D.B. Lovejoy, P.J. Jansson, U.T. Brunk, J. Wong, P. Ponka, D.R. Richardson, Antitumor activity of metal-chelating compound Dp44mT is mediated by

formation of a redox-active Cu complex that accumulates in lysosomes, Cancer Res. 71 (17) (2011) 5871–5880.

[16] J. Wang, F. Guo, M. Yu, L. Liu, F. Tan, R. Yan, N. Li, Rapamycin/DiR loaded lipid-polyaniline nanoparticles for dual-modal imaging guided enhanced photothermal and antiangiogenic combination therapy, J Control. Release 237 (2016) 23–34.

[17] F.F. Kabbinavar, H.I. Hurwitz, J. Yi, S. Sarkar, O. Rosen, Addition of bevacizumab to fluorouracil-based first-line treatment of metastatic colorectal cancer: pooled analysis of cohorts of older patients from two randomized clinical trials, J. Clin. Oncol. 27 (2009) 199–205.

[18] D.J. Slamon, B. Leyland-Jones, S. Shak, H. Fuchs, V. Paton, A. Bajamonde, T. Fleming, W. Eiermann, J. Wolter, M. Pegram, J. Baselga, L. Norton, Use of chemotherapy plus a monoclonal antibody against HER2 for metastatic breast cancer that overexpresses HER2, N. Engl. J. Med. 344 (2001) 783–792.

[19] W.H. Daly, D. Poché, The preparation of *N*-carboxyanhydrides of α-amino acidsusing bis(trichloromethyl)carbonate, Tetrahedron Lett. 29 (46) (1988) 5859–5862.

[20] M. Tanaka, M. Nakamura, T. Ikeda, K. Ikeda, H. Ando, Y. Shibutani, S. Yajima, K. Kimura, J. Org. Chem. 66 (2001)7008–7012.

[21] A. Samanta, M. Vendrell, R. Das, Y.T. Chang, Development of photostable near-infrared cyanine dyes, Chem. Commun. 46 (2010) 7406–7408.

[22] X. Cao, W. Lin, W. Wan, Development of a near-infrared fluorescent probe for imaging of endogenous Cu^{+} in live cells, Chem. Commun. 48 (2012) 6247–6249.

[23] T. Sun, Q. Guo, C. Zhang, J. Hao, P. Xing, J. Su, S. Li, A. Hao, G. Liu, Self-assembled vesicles prepared from amphiphilic cyclodextrins as drug carriers, Langmuir 28 (2012) 8625–8636.

[24] https://www.macrocyclics.com/online-catalog/macrocyclic-ligands, access data: 2 Dec. 2019.

[25] G.J. Brewer, R.D. Dick, D.K. Grover, V. LeClaire, M. Tseng, M. Wicha, K. Pienta, B.G. Redman, T. Jahan, V.K. Sondak, M. Strawderman, G. LeCarpentier, S.D. Merajver, Treatment of metastatic cancer with tetrathiomolybdate, an anticopper, antiangiogenic agent: phase I study, Clin. Cancer Res. 6 (2000) 1–10.

[26] N. Kitajima, Y. Morooka, Copper dioxygen complexes. Inorganic and bioinorganic perspectives. Chem. Rev. 94 (1994) 737–757.

[27] C. Vulpe, B. Levinson, S. Whitney, S. Packman, J. Gitschier, Isolation of a candidate gene for Menkes disease and evidence that it encodes a copper–transporting ATPase, Nat. Genet. 3 (1993) 7–13.

[28] P.C. Bull, G.R. Thomas, J.M. Rommens, J.R. Forbes, D.W. Cox, The Wilson disease gene is a putative copper transporting P–type ATPase similar to the Menkes gene, Nat. Genet. 5 (1993) 327–337.

[29] E.D. Harris, S.S. Percival, A role of ascorbic acid in copper transport, Am. J. Clin. Nutr. 54 (1991) 1193S–1197S.

[30] T. Sun, G. Zhang, Q. Wang, Z. Guo, Q. Chen, X. Chen, Y. Lu, Y. Zhang, Y. Zhang, Q. Guo, X. Gao, Y. Cheng, C. Jiang, Pre-blocked molecular shuttle as an in-situ

real-time theranostics, Biomaterials 204 (2019) 46–58.
[31] M.R. Eftink, M.L. Andy, K. Bystrom, H.D. Perlmutter, D.S. Kristol, Cyclodextrin inclusion complexes: studies of the variation in the size of alicyclic guests, J. Am. Chem. Soc. 111 (1989) 6765–6772.
[32] K. Pu, A.J. Shuhendler, J.V. Jokerst, J. Mei, S.S. Gambhir, Z. Bao, J. Rao, Semiconducting polymer nanoparticles as photoacoustic molecular imaging probes in living mice, Nat. Nanotechnol. 9 (2014) 233–239.
[33] L. Zeng, G. Ma, H. Xu, J. Mu, F. Li, X. Gao, Z. Deng, J. Qu, P. Huang, J. Lin, In vivo chemoselective photoacoustic imaging of copper(II) in plant and animal subjects, Small 15 (2019) 1803866.
[34] L. Yuan, W. Lin, S. Zhao, W. Gao, B. Chen, L. He, S. Zhu, A unique approach to development of near-infrared fluorescent sensors for in vivo imaging, J. Am. Chem. Soc. 134 (2012) 13510–13523.
[35] T. Mizuno, K. Mohri, S. Nasu, K. Danjo, H. Okamoto, Dual imaging of pulmonary delivery and gene expression of dry powder inhalant by fluorescence and bioluminescence, J. Control. Release 134 (2009) 149–154.
[36] S. Wang, Z. Sheng, Z. Yang, D. Hu, X. Long, C. Deng, Y. Liu, Z. Yuan, J. Zhang, H. Zheng, X. Zhang, Activatable small-molecule photoacoustic probes that cross the blood–brain barrier for visualization of copper(II) in mice with Alzheimer's Disease, Angew. Chem. Int. Ed. 58 (2019) 12415–12419.
[37] J. Wang, C. Luo, C. Shan, Q. You, J. Lu, S. Elf, Y. Zhou, Y. Wen, J.L. Vinkenborg, J. Fan, H. Kang, R. Lin, D. Han, Y. Xie, J. Karpus, S. Chen, S. Ouyang, C. Luan, N. Zhang, H. Ding, M. Merkx, H. Liu, J. Chen, H. Jiang, C. He, Inhibition of human copper trafficking by a small molecule significantly attenuates cancer cell proliferation, Nat. Chem. 7 (2015) 968–979.
[38] J. Esquivel, Technology of hyperthermic intraperitoneal chemotherapy in the United States, Europe, China, Japan, and Korea, Canc. J. 15 (2009) 249–254.
[39] Y. Zhao, E.B. Butler, M. Tan, Targeting cellular metabolism to improve cancer therapeutics, Cell Death Dis. 4 (2013) e532.
[40] G.J. Brewer, Zinc and tetrathiomolybdate for the treatment of Wilson's disease and the potential efficacy of anticopper therapy in a wide variety of diseases, Metallomics 1 (2009) 199–206.
[41] W. Song, Z. Tang, N. Shen, H. Yu, Y. Jia, D. Zhang, J. Jiang, C. He, H. Tian, X. Chen, Combining disulfiram and poly(*L*-glutamic acid)-cisplatin conjugates for combating cisplatin resistance, J. Control. Release 231 (2016) 94–102.
[42] A. Gupte, R.J. Mumper, Elevated copper and oxidative stress in cancer cells as atarget for cancer treatment, Cancer Treat Rev. 35 (2009) 32–46.
[43] A. McMahon, W. Chen, F. Li, Old wine in new bottles: Advanced drug delivery systems for disulfiram-based cancer therapy, J. Control. Release, 319 (2020) 352–359.
[44] M. Farokhi, F. Mottaghitalab, M.R. Saeb, S. Thomas, Functionalized theranostic nanocarriers with bio-inspired polydopamine for tumor imaging and chemo-photothermal therapy, J. Control. Release, 309 (2019) 203–219.
[45] A.V. Biankin, S. Piantadosi, S.J. Hollingsworth, Patient-centric trials for

therapeutic development in precision oncology, Nature 526 (2015) 361–370.